

Understanding the mechanisms behind high glacial productivity in the southern Brazilian margin

Rodrigo da C. Portilho-Ramos^{1,2}; Tainã M. L. Pinho^{2,3}; Cristiano M. Chiessi³; Cátia F. Barbosa⁴

¹MARUM - Center for Marine Environmental Sciences, University of Bremen, Leobener Strasse, 28359 Bremen, Germany.

²Institute of Geosciences, University of São Paulo, Rua do Lago 562, CEP05508-080, São Paulo, Brazil.

³School of Arts, Sciences and Humanities, University of São Paulo, Rua Arlindo Bettio 1000, CEP03828-000, São Paulo, Brazil.

⁴Departamento de Geoquímica, Universidade Federal Fluminense, Rua Outeiro São João Baptista S/N, CEP24020-141, Niterói, Rio de Janeiro, Brazil.

Correspondence to: Portilho-Ramos, R.C (rcpramos@marum.de)

Abstract. This study explores the mechanisms behind the high glacial productivity in the southern Brazilian margin during the last 70 kyr using planktonic foraminifera assemblage and subsurface temperatures derived through the Modern Analogue Technique. We show that enhanced glacial productivity was driven by the synergy of two mechanisms operating in different seasons: (i) an enhanced productivity in the upwelling region during short austral summer events; and (ii) the persistent presence of the Plata Plume Water due to prolonged austral winter conditions. We suggest that the upwelling systems in the southern Brazilian margin were more productive during the last glacial period due to the enhanced Si supply for diatom production through high-Si thermocline waters preformed in the Southern Ocean. We hypothesize that orbital forcing did not have a major influence on changes in upwelling during the last glacial period. However, the more frequent northward intrusions of the Plata Plume Water were modulated by austral winter insolation at 60°S through changes in the strength of alongshore SW-winds. After the Last Glacial Maximum, the reduced Si content of thermocline waters decreased upwelling productivity, while lower austral winter insolation decreased the influence of the Plata Plume Water over the southern Brazilian margin, reducing regional productivity.

41 1. Introduction

42 Continental margins are regions of relatively high biological productivity and long-term carbon
43 storage due to high nutrient flux (i.e. continental discharge and upwelling) and shallow seafloor depths
44 (i.e. interception of sinking particulate organic matter) (Abrantes et al., 2016; Bianchi et al., 2005;
45 Brandini et al., 2018; Ito et al., 2016; Wang et al., 2015). The high biological productivity and exportation
46 of particulate organic carbon to the seafloor, the so-called “biological pump” (Turner, 2015), play a
47 paramount role in removing CO₂ from the atmosphere (Bianchi et al., 2005; Muller-Karger et al., 2005).
48 It is estimated that ca. 0.06Pg C yr⁻¹ is buried in continental margins accounting for >40% of the carbon
49 storage in the oceans (Muller-Karger et al., 2005). Opposing to this drawdown, the upwelling of CO₂-
50 rich thermocline waters along continental margins can release CO₂ to the atmosphere (Bianchi et al.,
51 2005; Ito et al., 2016). Thus, continental margins have a great potential to modulate the drawdown and
52 emission of atmospheric CO₂, influencing the Earth’s climate system.

53 The southwestern Atlantic (southern Brazilian margin – SBM) is generally an oligotrophic area
54 bathed by nutrient-poor, warm and salty tropical waters of the Brazil Current (BC) (Fig. 1). However,
55 upwelling zones and riverine discharge inject nutrients into the photic zone (Brandini et al., 2018;
56 Campos et al., 2000, 2013; Garcia and Garcia, 2008; Möller et al., 2008) resulting in confined areas and
57 seasons with higher concentration of phyto-zooplankton biomass (Brandini et al., 2014; Rodrigues et al.,
58 2014). During austral summer, upwelling zones are intensified due to the prevailing alongshore
59 northeasterly winds and the cyclonic meanders of the BC induced by the interaction of the current with
60 the morphology of the continental margin (Aguiar et al., 2014; Campos et al., 2000; Castelao et al.,
61 2004). Winter conditions of vigorous alongshore SW-winds and a relatively weakened BC, allow the
62 northward intrusion of low-salinity waters from the Plata River along the SBM (Garcia and Garcia, 2008;
63 Möller et al., 2008). Both processes increase local productivity and lead to distinct changes in planktonic
64 community (Brandini et al., 2014; Rodrigues et al., 2014), that are preserved in sea-floor sediments and
65 can be used to reconstruct changes in productivity in the SBM over time (Gu et al., 2017; Lessa et al.,
66 2017; Portilho-Ramos et al., 2015).

67 Previous paleoceanographic studies provide evidence for an extremely intense primary
68 productivity in the SBM probably related to an upwelling system during part of Marine Isotope Stage 5
69 (~90 – 130 kyr) forced by strengthened NE-winds and BC (Lessa et al., 2017; Portilho-Ramos et al.,
70 2015). During the last glacial period (Marine Isotope Stages 2-4, ~11.7 – 71 kyr), primary productivity
71 weakened but was still significantly higher than the one occurring in the Holocene (Portilho-Ramos et
72 al., 2015). It has been suggested that the upwelling systems of the SBM were reduced during the last
73 glacial period, and may have been limited to short intervals of the austral summer due the prolonged
74 winter-like conditions of prevalent alongshore SW-winds and frequent cold front passages (Portilho-
75 Ramos et al., 2015). However, high abundance of eutrophic dinoflagellate cysts suggests increased
76 primary productivity in the SBM during specific intervals of the last glacial period (Gu et al., 2017).
77 These high productivity periods would be triggered by the input of local (i.e. Itajaí River) and remote
78 riverine nutrient-rich freshwater (i.e. Plata River plume) (Gu et al., 2017). Additionally, a recent study
79 proposed that the periods of expansion and contraction of the upwelling zones of the SBM are modulated
80 by eccentricity (Lessa et al., 2017), providing yet another mechanism to explain the evolution of primary

81 productivity in the SBM. In summary, these studies show that different oceanographic mechanisms may
82 have triggered high primary productivity in the SBM over time. These mechanism are, however, poorly
83 understood.

84 Here we used records of planktonic foraminifera assemblage and associated subsurface
85 temperature reconstructions derived by the Modern Analogue Technique (MAT) from piston core JPC-
86 17 (27°52.73'S, 46°55.25'W) to understand the paleoceanographic processes controlling changes in
87 biological productivity in the SBM over the last 70 kyr. The comparison of our results to previously
88 published records from the SBM allowed us to recognize two different mechanisms modulating past
89 productivity changes over the last glacial-interglacial cycle.

90

91 **2. Regional setting**

92 The SBM is an oligotrophic margin under the influence of warm ($\geq 25^{\circ}\text{C}$) and salty ($\geq 35\text{psu}$)
93 Tropical Water that flows southward within the BC (Fig. 1). Interactions of the BC with the morphology
94 of the margin (i.e. changes in the orientation of the margin and the presence of a barrier represented by
95 the Abrolhos Bank) generates cyclonic meanders and eddies that bring cold ($\leq 20^{\circ}\text{C}$) and nutrient-rich
96 thermocline waters (South Atlantic Central Waters (SACW) to shallower depths where they are subjected
97 to alongshore NE-winds (Aguiar et al., 2014; Campos et al., 2000; Castelao et al., 2004; Rodrigues and
98 Lorenzetti, 2001). Once over the shelf, wind stress and the Ekman dynamics brings the SACW to the
99 surface creating mature upwelling zones in the SBM (Aguiar et al., 2014; Castelao et al., 2004). These
100 processes boost biological productivity in specific portions of the SBM such as off Vitória ($\sim 18^{\circ}\text{S}$), Cabo
101 Frio (22° – 23°S) and Cape Santa Marta (27° – 29°S) during the austral summer (Fig. 1). Marine sediment
102 core JPC-17 investigated in this study was collected off Cape Santa Marta (Fig. 1).

103 In the vicinity of Cape Santa Marta, local productivity is also enhanced by the injection of
104 nutrients from freshwater discharge of local (i.e. Itajaí River) and remote (i.e. Plata River and
105 Patos/Mirim Lagoon complex) sources (Garcia and Garcia, 2008; Möller et al., 2008). During the
106 summer (Fig. 1A), the upwelling favorable NE-winds and the strong BC block the northward penetration
107 of the Plata Plume Water (PPW) (at ca. 32°S) (Campos et al. 2013; Möller et al. 2008). During austral
108 winter (Fig. 1B), the weakened BC and the prevailing alongshore SW-winds increase the northward
109 intrusion (up to ca. 27°S) of the nutrient-rich, cold ($\leq 18^{\circ}\text{C}$) and low salinity ($\leq 33.5\text{psu}$) PPW (Campos
110 et al. 2013; Möller et al. 2008).

111 Both upwelling and freshwater inject large amounts of nutrients into the oligotrophic SBM,
112 modulating seasonally the biological productivity as well as plankton community in the region (Garcia
113 and Garcia, 2008; Rodrigues et al., 2014). In the vicinity of the Cape Santa Marta, diatoms are the
114 dominant group of phytoplankton, accounting for 29–90% of phytoplankton and 31–90% of the carbon
115 biomass during the summer upwelling, while dinoflagellates dominates the phytoplankton during the
116 winter intrusion of the PPW (Brandini et al., 2014).

117

118 **3. Material and methods**

119 Piston core KNR159-5-17JPC ($27^{\circ}52,73'\text{S}$ and $46^{\circ}55,25'\text{W}$) recovered 15 m from which the
120 uppermost 350 cm were investigated in this study. The core was raised from 1627 m water depth during

121 R/V KNORR cruise 159-5 from Woods Hole Oceanographic Institution (WHOI, USA) (Fig. 1). The
122 upper 350 cm of the core consist in dark gray carbonate sediments. This section was sampled
123 continuously every 10 cm and 2 g of sediment per sample were washed in 62 μm sieves.

124

125 **3.1. Planktonic foraminifera assemblage**

126 Planktonic foraminifera from core JPC-17 were dry picked from $>150 \mu\text{m}$ size fraction and
127 quantified in relative abundances from splits containing more than 300 specimens per sample. The
128 taxonomy was based on Stainforth et al., (1975). We assumed the effect of dissolution in our planktonic
129 foraminiferal faunal composition to be negligible since core JPC-17 was collected at 1627 m water depth,
130 well above the modern and glacial lysocline (Volbers and Henrich, 2004). Here we do not distinguish
131 between *Globigerinoides ruber* white and pink variety, and also counted *Globigerinoides sacculifer* and
132 *Globigerinoides trilobus* together as *G. sacculifer* since they are genetically the same species (André et
133 al., 2013). Considering the taxonomic ambiguity in distinguishing the small-sized (i.e. $\leq 250 \mu\text{m}$)
134 specimens of *Globigerinella calida* and *Globigerinella siphonifera* (Vargas et al., 2002) we counted
135 them together as *G. siphonifera*.

136

137 **3.2. Subsurface temperature reconstruction**

138 We reconstructed subsurface temperatures at 100 m water depth using the modern analog
139 technique (MAT) following Portilho-Ramos et al. (2015). The MAT was performed on the software C2
140 (Juggins, 2007) and the basic assumption is that temperature of ambient seawater is the primary control
141 of the foraminiferal assemblage (Morey et al., 2005). The planktonic foraminiferal calibration dataset
142 used here comprises 1052 surface samples from the Atlantic Ocean, from which 891 samples were
143 previously published in Kucera et al. (2005a) and 161 samples from North Atlantic eastern boundary
144 upwelling zones previously published in Salgueiro et al. (2014). The modern annual temperature values
145 at 100 m water depth from WOA 2009 (Locarnini et al., 2010) were extracted and used to calibrate the
146 MAT. For the MAT transfer function, the squared chord distance was applied as similarity measure.
147 Additionally, when reconstruction results were evaluated, the weighted mean of the best 10 modern
148 analogs was used (Kucera et al., 2005b). Using the leave-one-out cross-validation method, the root mean
149 square error of prediction of the transfer function is 0.95°C ($R^2 = 0.98$).

150

151 **3.3. Age model**

152 An age model for core JPC-17 has been previously published on the basis of calibrated
153 radiocarbon AMS ^{14}C ages, $\delta^{18}\text{O}$ in both planktonic and benthic foraminifera as well as regional
154 planktonic foraminifera biostratigraphy (Portilho-Ramos et al., 2014a; Tessin and Lund, 2013).
155 Reversals in radiocarbon ages from ca. 16 to 21 calibrated kiloannum before present (i.e. 1950 AD) (cal
156 ka BP) were detected by Tessin and Lund (2013). These authors excluded four radiocarbon ages (i.e. 50,
157 54, 58 and 82 cm core depth) out of 17 dated samples from core JPC-17 because of reversals (Table 1).
158 The radiocarbon age obtained at 56 cm from Portilho-Ramos et al., 2014a) is placed within this interval
159 and also seems to be reversed. Considering these age reversals, the chronology of the JPC-17 was
160 improved using the R script BACON version 2.2, which uses Bayesian statistics to reconstruct

161 accumulation histories for sedimentary deposits and considers a Student-t model to address outlying
162 (reversed) ages (Blaauw and Christen, 2011). Thus, as explained by Blaauw and Christen (2011),
163 BACON version 2.2 is not affected by outlying ages. For the upper 190 cm of core JPC-17, all AMS ^{14}C
164 ages (Table 1) were calibrated using the IntCal13 calibration curve (Reimer et al., 2013) with a reservoir
165 correction age of 400 ± 100 yr (1σ error). For the core section that extrapolates the radiocarbon range (i.e.
166 191 - 350 cm), two additional tie-points (Table 1) were obtained by aligning the benthic foraminifera
167 stable oxygen isotopes ($\delta^{18}\text{O}$) record from JPC-17 to benthic $\delta^{18}\text{O}$ of nearby core GL-1090 (Santos et al.,
168 2017) (Fig. 1) and to the intermediate-depth South Atlantic benthic $\delta^{18}\text{O}$ stack LS16 (Lisiecki and Stern,
169 2016) using the Analyseries 2.0.5.2 software (Paillard et al., 1996) (Fig. 2). The benthic $\delta^{18}\text{O}$ curve from
170 JPC-17 is a combination of published *Cibicidoides* spp. (Tessin and Lund, 2013) and unpublished
171 *Cibicidoides* spp. $\delta^{18}\text{O}$ provided by WHOI (Fig. 2). The latest follow the methodology applied in (Curry
172 and Oppo, 2005). Error estimations of the $\delta^{18}\text{O}$ tie-points followed Santos et al. (2017), which take into
173 account the mean resolution of the JPC-17 benthic $\delta^{18}\text{O}$ record around the tie-point depth, the mean
174 resolution of the reference curve around the tie-point age, a matching error visually estimated when
175 defining tie-points and the absolute age error of the time-scale used for the reference record. Beside the
176 default parameters of the software, the following settings were used: mem.mean = 0.4, acc.shape = 0.5.
177 and t.a =9/t.b =10. A total of 10,000 age-depth realizations have been used to calculate the median age
178 and the 1σ analytical uncertainty at 5 mm resolution (Fig. 2B). The chronology of core JPC-17 was
179 additionally supported by planktonic foraminifera biostratigraphy (Ericson and Wollin, 1968; Portilho-
180 Ramos et al., 2014b), where the presence of *Globorotalia menardii* and the low abundance of
181 *Globorotalia inflata* indicate Biozone Z (Holocene), while the absence of *G. menardii* and the high
182 abundance of *G. inflata* characterize the glacial Biozone Y (last glacial period) (Fig. 2).

183

184 4. Results

185 In contrast to a previous chronology (Portilho-Ramos et al., 2014a), the new age model for the
186 upper 350cm of core JPC-17 spans the last ca. 70 cal ka BP (Fig. 2). The benthic oxygen isotope records
187 from core JPC-17 display a clear glacial-interglacial pattern, comparable to the benthic $\delta^{18}\text{O}$ record of
188 nearby core GL-1090 as well as that of the intermediate-depth South Atlantic benthic $\delta^{18}\text{O}$ stack LS16
189 (Lisiecki and Stern, 2016) (Fig. 2).

190 Planktonic foraminifera assemblage is composed of 28 species and subspecies. The following
191 six species accounted for more than 70% of total planktonic assemblage: *G. ruber* (39%); *Globigerina*
192 *glutinata* (13%); *G. bulloides* (11.2%); *G. inflata* (8.8%); *G. sacculifer* (5%); and *G. siphonifera* (2.5%).
193 The abundance of *G. menardii* (0.7%), *Pulleniatina obliquiloculata* (0.3%), *Orbulina universa* (0.3%),
194 *Globorotalia crassaformis* (0.3%), *Neogloboquadrina dutertrei* (5.5%) and *Globorotalia*
195 *truncatulinoidea* (3.9%) were published in Portilho-Ramos et al., (2014a).

196 In general, the distribution of the most abundant species follows the glacial-interglacial pattern
197 over the last 70 kyr (Fig. 3). The abundance of the non-spinose species *G. bulloides* and *G. inflata* were
198 higher during the last glacial period (mean of 12% and 9.6%, respectively) and lower during the Holocene
199 (mean of 4.6% and ~2%, respectively) (Fig. 3A, 3B, respectively). In contrast, the abundance of spinose
200 species displayed the opposite behavior. The abundance of *G. ruber* ranged from 25 to 50% (mean of

201 39%) during the glacial and increased after 40 cal ka BP towards the Holocene (mean of 47) (Fig. 3C).
202 The abundance of *G. sacculifer* and *G. siphonifera* display similar patterns (Fig. 3D, E, respectively),
203 and ranged between 1.6–10.4% and 0–7.6% (respectively), with higher abundance during the postglacial
204 interval (mean of 7.5 and 6.9%, respectively).

205 The temperature at 100 m-water depth derived from MAT ranged from 16°C to 21.3°C over the
206 last 70 kyr with lower temperatures recorded during the glacial (16°–20.3°C) in comparison to the
207 Holocene (~21°C) (Fig. 3F). A pronounced warming trend is observed after 30 cal ka BP toward the
208 Holocene.

209

210 5. Discussion

211 Planktonic foraminifera *G. bulloides* is a non-spinose surface-dwelling species generally
212 inhabiting regions of cold and high phytoplankton biomass typically associated with upwelling zones
213 (Lessa et al., 2014; Mohtadi et al., 2007; Sautter and Thunell, 1991). Thus, high abundances of *G.*
214 *bulloides* in marine sediments from regions potentially affected by upwelling have been widely used as
215 an upwelling indicator (Godad et al., 2011; Peeters et al., 2002), including the SBM upwelling zones
216 (Lessa et al., 2017; Portilho-Ramos et al., 2015). The last glacial abundance of *G. bulloides* in core JPC-
217 17 (8–18%) (Fig. 3A) closely matches those found in surface sediments from the Cabo Frio upwelling
218 (10–20%) (Lessa et al., 2014), suggesting the occurrence of a sustained upwelling off Cape Santa Marta
219 in the SBM. It also closely matches glacial records from cores collected further north at the SBM such
220 as GL-75 (21°83'S; 40°01'W) (Portilho-Ramos et al., 2015), GL-77 (21°12'S; 40°02'W) (Petró et al.,
221 2016) and SAN 76 (24°26'S; 42°17'W) (Toledo et al., 2007), where *G. bulloides* ranged between 8%–
222 17%, suggesting widespread cooling and elevated productivity at the SBM during the last glacial period
223 relative to the modern oligotrophic conditions (Fig. 4A, B). During the last glacial period, the reduced
224 abundance of non-upwelling species *G. ruber* (25–50%) and other warm and oligotrophic symbiont-
225 bearing species like *G. sacculifer* (2.1–10.4%) and *G. siphonifera* (0.3%–4.3%) (Fig. 3) support the
226 occurrence of cold-productive conditions promoted by upwelling. Simultaneously, lower temperatures
227 at 100 m water depth ($\leq 20^{\circ}\text{C}$) suggest that SACW may have been frequently located in the photic zone.
228 The isotherm of 20°C is used to track the boundary between Tropical Water and SACW (Castelao et al.,
229 2004), and has been used as a proxy for the presence of SACW in the photic zone in the past (Portilho-
230 Ramos et al., 2015; Lessa et al., 2017). It should be highlighted that a relative warming of thermocline
231 waters observed after 30cal ka BP may be related to heat accumulation in the western South Atlantic
232 associated to the glacial reduced mode of the Atlantic meridional overturning circulation (Santos et al.,
233 2017) as well as increased transport of heat from Indian Ocean into South Atlantic through Agulhas
234 Leakage (Martínez-Méndez et al., 2010).

235 Enhanced glacial productivity in the SBM was recently reported by a 74 kyr-long record of
236 dinoflagellate cysts from adjacent core GeoB2107-3 (27°17'S; 46°45'W) (Gu et al., 2007). The authors
237 provide evidences for increased eutrophic conditions associated to more frequent northward intrusions
238 of the PPW (Fig. 4D) (Gu et al., 2017). However, *G. bulloides* is virtually absent in surface sediments
239 deposited under the influence of the PPW to the north from the Brazil-Malvinas Confluence (Chiessi et
240 al., 2007). Thus, more frequent northward penetrations of the PPW in our study site is unlikely to explain

241 the enhanced glacial abundance of *G. bulloides*. In addition, the abundance of the eutrophic
242 environmental dinocysts and *G. bulloides* show different behavior along the last glacial period (Fig. 4A,
243 D). The dinocysts increased in abundance between 54–74 cal ka BP and 14–40 cal ka BP, suggesting
244 increased productivity related to frequent northward intrusions of the PPW, while the opposite is
245 observed between 40–54 cal ka BP (Fig. 4D), suggesting reduced influence of the PPW and relatively
246 low productivity (Gu et al., 2017). In contrast, the abundance of the *G. bulloides* remained relatively high
247 during the entire glacial with a decrease trend after 30 cal ka BP toward the Holocene (Figs. 3A, 4B).
248 Furthermore, enhanced abundance of *G. bulloides* during the last glacial period is also observed as far
249 north as 21°S (i.e. core GL-75) (Fig. 4A) (Portilho-Ramos et al., 2015), which is unlikely be explained
250 by continuous presence of the PPW (Möller et al., 2008).

251

252 **5.1. Modern and past seasonal productivity processes in the SBM**

253 Modern surface productivity in the SBM is seasonally modulated by two different processes
254 that inject nutrients in the photic zone: (i) austral summer coastal and shelf-break upwelling (Campos et
255 al., 2013); and (ii) austral winter northward intrusions of the PPW (Garcia and Garcia, 2008; Möller et
256 al., 2008). During austral summer upwelling events, diatoms are the dominant group of the
257 phytoplankton, accounting for 29–90% of phytoplankton density and 31–90% of the carbon biomass,
258 while dinoflagellate is the dominant group during the austral winter associated to northward intrusions
259 of the PPW (Brandini et al., 2014). We suggest that both taxa reveal different seasonal conditions during
260 the last glacial period, with *G. bulloides* recording upwelling events during austral summer and
261 dinoflagellate recording northward intrusions of the PPW during austral winter.

262 Prolonged winter-like conditions of prevalent alongshore SW-winds and frequent cold front
263 passages during the last glacial period may have limited the SBM upwelling systems to a short period of
264 austral summer-like conditions, as suggested by Portilho-Ramos et al. (2015). Furthermore, increased
265 continental runoff (i.e. Itajaí River, Plata River and Patos/Mirim Lagoon complex) associated with
266 enhanced precipitation over SE South America (Cruz et al., 2005; Wang et al., 2007) as well as a vigorous
267 alongshore SW-winds were favorable to the northward penetration of the PPW. These conditions
268 increased the abundance of dinocysts characteristic of eutrophic conditions in the SBM during the glacial
269 (Gu et al., 2017). The lower sea level (Waelbroeck et al., 2002) may have caused offshore displacement
270 of the PPW over to our core site location (Lantzsch et al., 2014).

271 Importantly, our reconstructed temperature at 100 m water depth indicates that SACW may
272 have reached the photic zone during the last glacial period (Fig. 3F). Modern hydrographic data and
273 model simulations show that shelf-break upwelling in the SBM induced by the interaction of the BC with
274 bottom topography occurs year-long but is modulated by seasonal alongshore-wind direction (Brandini
275 et al., 2018; Campos et al., 2013). Thus, a prolonged presence of the low salinity PPW in the region may
276 have increased the upper water stratification and suppressed the surfacing of SACW, favoring the
277 proliferation of eutrophic dinocysts. In contrast, during short austral summer periods, the strengthening
278 of both the alongshore NE-winds and the BC hampered the northward PPW migration, inducing the
279 upwelling of SACW and creating favorable conditions to the proliferation of *G. bulloides*. Owing to the
280 low resolution of core JPC-17, we cannot rule out an antiphase between the *G. bulloides* (i.e. core JPC-

281 17) and the dinocyst (i.e. core GeoB2107-3) records that would assign the SW-winds and the associated
282 northward penetration of PPW a key role on controlling the upwelling zones in the SBM during the last
283 glacial period.

284

285 **5.2. Orbital forcing of SBM upwelling systems**

286 A recent study proposed orbitally forced changes in insolation (eccentricity) as a major
287 mechanism modulating the intensification/deintensification as well as the expansion/contraction
288 dynamics of the SBM upwelling zones (Lessa et al., 2017). In accordance to these authors, eccentricity
289 maximum (≥ 0.03) during MIS5 would have altered the seasonality of the wind regime by controlling
290 the amplitude of austral summer and winter insolation and the South Atlantic subtropical high-pressure
291 position. Thus, prolonged NE-winds during austral summer promoted intensification and expansion
292 (from 24°S to 28°S) of the SE-Brazil upwelling systems during MIS5. On the other hand, eccentricity
293 minimum (≤ 0.02) during the Holocene would result in weak NE-winds and deintensifying and
294 contracting these upwelling systems in comparison to MIS5 (Lessa et al., 2017).

295 However, the orbital mechanism proposed by Lessa et al. (2017) does not explain the
296 intensified/expanded upwelling in the SBM during the last glacial period, since eccentricity was ≤ 0.02
297 during the entire interval (Fig. 4C). Interestingly, the dinocyst record from core GeoB2107-3 matches
298 austral winter (June) insolation at 60°S very well over the last 70 kyr (Fig. 4D), highlighting the close
299 connection between dinocyst abundance and winter conditions through vigorous alongshore SW-winds
300 and increased presence of the PPW in our core site. Periods of increased austral winter insolation at 65°S
301 may have steeped the thermal gradient between the high and mid latitudes in the Atlantic sector of the
302 Southern Ocean, intensifying the alongshore SW-wind system and the northward incursion of PPW,
303 thereby boosting the eutrophic environmental dinocyst productivity in the SBM.

304

305 **5.3. The silicic acid leakage hypothesis (SALH)**

306 In sections 5.1 and 5.2, we showed that *G. bulloides* and dinocysts record different seasonal
307 productivity processes in the SMB. While austral winter productivity events were triggered by the more
308 frequent northward intrusions of the PPW, it is not clear what could explain the occurrence of austral
309 summer productivity events related to upwelling in the SBM.

310 We suggest that, rather than being driven by changes in upwelling intensity as observed during
311 interglacial MIS5 (Lessa et al., 2017; Portilho-Ramos et al., 2015), the increased productivity may have
312 been a result of increased silicic acid (Si(OH)_4) content supplied by the glacial SACW. Several
313 paleorecords and model experiments addressed the hypothesis of increased export of dissolved Si(OH)_4
314 preformed in the Southern Ocean that have fueled primary diatom productivity in low latitude upwelling
315 zones and continental margins during the last glacial period, the so called “silicic acid leakage
316 hypothesis” (SALH) (Bradtmitter et al., 2007; DeMaster, 2002; Matsumoto et al., 2014; Sarmiento et al.,
317 2004). The SALH postulates that during glacial periods, imposed sea ice around Antarctica displaced the
318 zone of high diatom production to the North of the Antarctic Polar Front (APF), where thermocline
319 waters (i.e. Subantarctic Mode Water, a precursor of SACW and Antarctic Intermediate Water - AAIW)
320 are formed (Abelmann et al., 2015; Bradtmiller et al., 2007; Sarmiento et al., 2004). Thus, (unused) high-

321 Si waters were exported from the Southern Ocean to the low latitude world ocean, where diatom
322 production increased at the expense of other types of phytoplankton (Bradt Miller et al., 2007; Griffiths
323 et al., 2013; Sarmiento et al., 2004). In the Brazilian margin, the silicon isotopic composition ($\delta^{30}\text{Si}$) of
324 sponge spicules from nearby core GeoB2107-3 indicates no substantial difference in the $\text{Si}(\text{OH})_4$ content
325 of AAIW between the Last Glacial Maximum and the Holocene, which would contradict the SALH
326 (Hendry et al., 2012). However, high $\text{Si}(\text{OH})_4$ pulses that occurred during the Younger Dryas and
327 Heinrich Stadials (Hendry et al., 2012) make the $\text{Si}(\text{OH})_4$ content of the average last glacial AAIW higher
328 than that of the average Holocene AAIW. Significant increment of $\text{Si}(\text{OH})_4$ transported by AAIW was
329 also observed in the western equatorial Atlantic at the onset of the last glacial (40–80 cal ka BP), which
330 was not followed by enhanced surface productivity indicating that AAIW $\text{Si}(\text{OH})_4$ did not reach the
331 photic zone (Griffiths et al., 2013). However, equatorial Atlantic upwelling zones are fed by SACW and
332 high glacial opal burial as a consequence of enhanced surface diatoms production due to intense
333 upwelling is considered a direct evidence from the SALH (Bradt Miller et al., 2007). Indeed, SACW is
334 the major conduit for sub-Antarctic thermocline waters involved in SALH (Sarmiento et al., 2004) and
335 bear a great potential to boost primary production in the SBM (Campos et al., 2000).

336 Currently, diatoms dominate the phytoplankton in the SBM during austral summer SACW
337 upwelling (Brandini et al., 2014) and are an important component of the diet of the symbiotic-barren *G.*
338 *bulloides*, which can alternatively feed on zooplankton (i.e. copepods) (Sautter and Thunell, 1991;
339 Schiebel and Hemleben, 2017; Thunell and Sautter, 1992). Within age model uncertainties (including
340 also the radiocarbon reversals in our core) and considering the different temporal resolution of the
341 records, the glacial high abundance of *G. bulloides* in core JPC-17 matches well with high biogenic
342 Opal% in cores RC24-01 and RC24-07 from the equatorial upwelling off NW-Africa (Bradt Miller et al.,
343 2007) as well as core RC13-254, to the north of the APF Front (Atlantic sector) (Mortlock et al., 1991)
344 (Fig. 4B, F and G). It is noteworthy that SACW also receives contributions from the Indian Ocean
345 through the Agulhas Leakage (warm water route; Donners and Drijfhout, 2004), where the production
346 of opal (north of the APF) and export of silicic acid remained high over the entire last glaciation (Dezileau
347 et al., 2003). We suggest that *G. bulloides* in the SBM may have benefited the silicic acid-induced diatom
348 blooms by directly feeding diatoms and/or indirectly by preying other zooplankton that also feed on
349 diatoms. Thus, the increased abundance of *G. bulloides* in the SBM during the last glacial period was
350 related to upwelling-driven high productivity during short austral summer periods, as previously
351 suggested in Portilho-Ramos et al. (2015). In contrast, prolonged austral winter conditions with vigorous
352 alongshore SW-winds as well as increased precipitation over SE South America (Cruz et al., 2005; Wang
353 et al., 2007) increased the northward penetration of the PPW leading to enhanced eutrophic
354 environmental dinocyst productivity during the last glaciation (Gu et al., 2017). Taken together, both
355 processes may have boosted biological primary productivity along the year during the last glacial period.
356 This is supported by enhanced abundance of deep-dwelling herbivorous planktonic foraminifera species
357 *Globorotalia inflata* (Schiebel and Hemleben, 2017) that calcifies between 200 and 400 m water depth
358 (Chiessi et al., 2007) and would have benefited by grazing the increased amount of sinking organic
359 particles.

360

361 5.4. Post-glacial conditions

362 After the Last Glacial Maximum, the abundance of *G. bulloides* and eutrophic dinocysts
363 decrease until the onset of the Holocene, suggesting decreased regional productivity and more
364 oligotrophic conditions in comparison to the last glacial period (Fig. 4B, D). The presence of oligotrophic
365 conditions is supported by increased abundance of tropical symbiont-bearing species *G. ruber* (37–52%),
366 *G. sacculifer* (6–8.8%) and *G. siphonifera* (6.3–7.5%) (Fig. 3). The low abundance of *G. inflata* also
367 suggests oligotrophic conditions during the Holocene (Fig. 3B). Despite the favorable conditions for
368 upwelling in the SBM during the Holocene (i.e. occurrence of alongshore NE-winds and a strong BC;
369 Chiessi et al., 2014; Lessa et al., 2017; Portilho-Ramos et al., 2015), upwelling productivity may have
370 been hampered by the reduced export of pre-formed silicic acid through SACW (Fig. 4F, G). This is
371 supported by the substantial decrease of biogenic opal in equatorial upwelling cores RC24-01 and RC24-
372 07 after 15 cal ka BP (Fig. 4F; Bradtmiller et al., 2007). Indeed, the retraction of Antarctic sea ice
373 displaced the zone of enhanced biogenic opal production to the south of the APF, retaining the excess of
374 silicic acid and opal burial in the Southern Ocean (Bradtmiller et al., 2007; Sarmiento et al., 2004) as
375 evidenced by increased Holocene biogenic opal to the South of the APF at core RC13-259 (Fig. 4G;
376 Mortlock et al., 1991). In addition, low austral winter insolation at 65°S and reduced sea ice may have
377 decrease the thermal gradient between the high and mid latitudes in the Atlantic sector of the Southern
378 Ocean and consequently weakened the alongshore SW-winds in the SBM, inhibiting the northward
379 intrusions of the PPW. Simultaneously, the high sea level stand modified the SBM morphology
380 increasing the width of the southern Brazilian shelf and, displacing the core of the upwelling zone to the
381 inner shelf off Cape Santa Marta where it is controlled by local factors such as coastal wind system
382 (Campos et al., 2013; Möller et al., 2008). The high temperatures at 100 m water depth from core JPC-
383 17 (Fig. 3F) support this hypothesis, suggesting that the SACW was not frequently in the photic zone at
384 the core location.

385

386 6. Conclusions

387 In this study we used planktonic foraminifera assemblage and associated 100 m water depth
388 temperatures to discuss changes in productivity in the southern Brazilian margin over the last 70 kyr.
389 The enhanced abundance of upwelling indicator *Globigerina bulloides* (12–16%) together with the
390 reduced abundance of oligotrophic species and subsurface temperatures lower than 20°C suggest the
391 occurrence of upwelling off Cape Santa Marta during the last glacial period. We suggest that rather than
392 being driven by changes in upwelling intensity, the increased productivity may have been a result of
393 increased silicic acid export from the Southern Ocean through South Atlantic Central Water. Our results
394 show that orbital forcing did not have a major influence on changes in upwelling during the last glacial
395 period. We further show that more frequent northward intrusions of Plata Plume Water modulated by
396 austral winter insolation at 65°S through enhanced alongshore SW-winds boosted austral winter
397 productivity at the SBM. Thus, a productive upwelling during short austral summer events and the
398 prolonged presence of Plata Plume Water during austral winter enhanced the biological productivity
399 year-round in the SBM during the last glacial period relative to modern conditions. After the Last Glacial
400 Maximum, low silicic acid content in thermocline waters decreased the productivity of the upwelling,

401 while lower austral winter insolation at 65°S and associated weakened SW-winds reduced the presence
402 of the Plata Plume Water in the SBM. In addition, last deglaciation sea level rise may have modified the
403 geomorphology of the SBM limiting the upwelling system to the coast, southern to Cape Santa Marta.

404

405 **Acknowledgments.** We thank two anonymous Referees for their constructive comments. We are
406 grateful to Delia Oppo and William B. Curry from Woods Hole Oceanographic Institute, United States,
407 for providing the oxygen isotope data from core JPC-17 used here. R.C.P.-R. thanks PNPd scholarship
408 from CAPES. T.M.L.P. thanks PIBIC scholarship from CNPq (2017-482). C.M.C. acknowledges the
409 financial support from FAPESP (grant 2012/17517-3), CAPES (grants 1976/2014 and 564/2015) and
410 CNPq (grants 302607/2016-1 and 422255/2016-5).

411

412 **Data availability.** The data reported here will be archived in in the World Data Center PANGAEA
413 (www.pangaea.de).

414

415 **Author contributions**

416 R.C.P.-R. and C.M.C. designed the study. R.C.P.-R. and T.M.L.P. analyzed planktonic foraminifera
417 assemblage. R.C.P.-R. and C.M.C. wrote the manuscript. R.C.P.-R. performed the Modern Analogue
418 Technique. R.C.P.-R. and C.F.B performed age modeling. All authors contributed to the interpretation
419 of the data.

420

421 **Competing interests.** The authors declare that they have no conflict of interest.

422

423 **7. References**

424 Abelmann, A., Gersonde, R., Knorr, G., Zhang, X., Chaplignin, B., Maier, E., Esper, O., Friedrichsen,
425 H., Lohmann, G., Meyer, H. and Tiedemann, R.: The seasonal sea-ice zone in the glacial
426 Southern Ocean as a carbon sink, *Nat. Commun.*, 6(1), 8136, doi:10.1038/ncomms9136, 2015.

427 Abrantes, F., Cermeno, P., Lopes, C., Romero, O., Matos, L., Van Iperen, J., Rufino, M. and
428 Magalhães, V.: Diatoms Si uptake capacity drives carbon export in coastal upwelling systems,
429 *Biogeosciences*, 13(14), 4099–4109, doi:10.5194/bg-13-4099-2016, 2016.

430 Aguiar, A. L., Cirano, M., Pereira, J. and Marta-Almeida, M.: Upwelling processes along a western
431 boundary current in the Abrolhos-Campos region of Brazil, *Cont. Shelf Res.*, 85, 42–59,
432 doi:10.1016/j.csr.2014.04.013, 2014.

433 André, A., Weiner, A., Quillévéré, F., Aurahs, R., Morard, R., Douady, C. J., de Garidel-Thoron, T.,
434 Escarguel, G., de Vargas, C. and Kucera, M.: The cryptic and the apparent reversed: lack of
435 genetic differentiation within the morphologically diverse plexus of the planktonic foraminifer
436 *Globigerinoides sacculifer*, *Paleobiology*, 39(01), 21–39, doi:10.1666/0094-8373-39.1.21, 2013.

437 Bianchi, A. A., Bianucci, L., Piola, A. R., Pino, D. R., Schloss, I., Poisson, A. and Balestrini, C. F.:
438 Vertical stratification and air-sea CO₂ fluxes in the Patagonian shelf, *J. Geophys. Res.*, 110(C7),
439 1–10, doi:10.1029/2004JC002488, 2005.

440 Blaauw, M. and Christen, J. A.: Flexible paleoclimate age-depth models using an autoregressive

441 gamma process, *Bayesian Anal.*, 6, 457–474, doi:10.1214/11-BA618, 2011.

442 Bradtmiller, L. I., Anderson, R. F., Fleisher, M. Q. and Burckle, L. H.: Opal burial in the equatorial
443 Atlantic Ocean over the last 30 ka: Implications for glacial-interglacial changes in the ocean
444 silicon cycle, *Paleoceanography*, 22(4), PA4216, doi:10.1029/2007PA001443, 2007.

445 Brandini, F. P., Nogueira, M., Simião, M., Codina, J. C. U. and Almeida Noernberg, M.: Deep
446 chlorophyll maximum and plankton community response to oceanic bottom intrusions on the
447 continental shelf in the South Brazilian Bight, *Cont. Shelf Res.*, 89, 61–75,
448 doi:10.1016/j.csr.2013.08.002, 2014.

449 Brandini, F. P., Tura, P. M. and Santos, P. P. G. M.: Ecosystem responses to biogeochemical fronts in
450 the South Brazil Bight, *Prog. Oceanogr.*, 164(April), 52–62, doi:10.1016/j.pocean.2018.04.012,
451 2018.

452 Campos, E. J. D., Velhote, D. and da Silveira, I. C. A.: Shelf break upwelling driven by Brazil Current
453 Cyclonic Meanders, *Geophys. Res. Lett.*, 27(6), 751–754, doi:10.1029/1999GL010502, 2000.

454 Campos, P. C., Möller, O. O., Piola, A. R. and Palma, E. D.: Seasonal variability and coastal upwelling
455 near Cape Santa Marta (Brazil), *J. Geophys. Res. Ocean.*, 118(3), 1420–1433,
456 doi:10.1002/jgrc.20131, 2013.

457 Castelao, R. M., Campos, E. J. D. and Miller, J. L.: A Modelling Study of Coastal Upwelling Driven
458 by Wind and Meanders of the Brazil Current, *J. Coast. Res.*, 203, 662–671, doi:10.2112/1551-
459 5036(2004)20[662:AMSOCU]2.0.CO;2, 2004.

460 Chiessi, C. M., Ulrich, S., Mulitza, S., Pätzold, J. and Wefer, G.: Signature of the Brazil-Malvinas
461 Confluence (Argentine Basin) in the isotopic composition of planktonic foraminifera from
462 surface sediments, *Mar. Micropaleontol.*, 64(1–2), 52–66, doi:10.1016/j.marmicro.2007.02.002,
463 2007.

464 Chiessi, C. M., Mulitza, S., Groeneveld, J., Silva, J. B., Campos, M. C. and Gurgel, M. H. C.:
465 Variability of the Brazil Current during the late Holocene, *Palaeogeogr. Palaeoclimatol.*
466 *Palaeoecol.*, 415, 28–36, doi:10.1016/j.palaeo.2013.12.005, 2014.

467 Cruz, F. W., Burns, S. J., Karmann, I., Sharp, W. D., Vuille, M., Cardoso, A. O., Ferrari, J. A., Dias, P.
468 L. S. and Viana, O.: Insolation-driven changes in atmospheric circulation over the past 116,000
469 years in subtropical Brazil., *Nature*, 434(7029), 63–6, doi:10.1038/nature03365, 2005.

470 Curry, W. B. and Oppo, D. W.: Glacial water mass geometry and the distribution of $\delta^{13}\text{C}$ of ΣCO_2 in
471 the western Atlantic Ocean, *Paleoceanography*, 20(1), n/a-n/a, doi:10.1029/2004PA001021, 2005.

472 DeMaster, D. J.: The accumulation and cycling of biogenic silica in the Southern Ocean: Revisiting the
473 marine silica budget, *Deep. Res. Part II Top. Stud. Oceanogr.*, 49(16), 3155–3167,
474 doi:10.1016/S0967-0645(02)00076-0, 2002.

475 Dezileau, L., Reyss, J. L. and Lemoine, F.: Late Quaternary changes in biogenic opal fluxes in the
476 Southern Indian Ocean, *Mar. Geol.*, 202(3–4), 143–158, doi:10.1016/S0025-3227(03)00283-4,
477 2003.

478 Donners, J. and Drijfhout, S. S.: The Lagrangian View of South Atlantic Interocean Exchange in a
479 Global Ocean Model Compared with Inverse Model Results, *J. Phys. Oceanogr.*, 34(5), 1019–
480 1035, doi:10.1175/1520-0485(2004)034<1019:TLVOSA>2.0.CO;2, 2004.

481 Ericson, D. B. and Wollin, G.: Pleistocene Climates and Chronology in Deep-Sea Sediments, *Science*
482 (80-.), 162(3859), 1227–1234, doi:10.1126/science.162.3859.1227, 1968.

483 Garcia, C. A. E. and Garcia, V. M. T.: Variability of chlorophyll-a from ocean color images in the La
484 Plata continental shelf region, *Cont. Shelf Res.*, 28(13), 1568–1578,
485 doi:10.1016/j.csr.2007.08.010, 2008.

486 Godad, S. P., Naidu, P. D. and Malmgren, B. A.: Sea surface temperature changes during May and
487 August in the western Arabian Sea over the last 22kyr: Implications as to shifting of the
488 upwelling season, *Mar. Micropaleontol.*, 78(1–2), 25–29, doi:10.1016/j.marmicro.2010.09.006,
489 2011.

490 Griffiths, J. D., Barker, S., Hendry, K. R., Thornalley, D. J. R., van de Flierdt, T., Hall, I. R. and
491 Anderson, R. F.: Evidence of silicic acid leakage to the tropical Atlantic via Antarctic
492 Intermediate Water during Marine Isotope Stage 4, *Paleoceanography*, 28(2), 307–318,
493 doi:10.1002/palo.20030, 2013.

494 Gu, F., Zonneveld, K. A. F., Chiessi, C. M., Arz, H. W., Pätzold, J. and Behling, H.: Long-term
495 vegetation, climate and ocean dynamics inferred from a 73,500 years old marine sediment core
496 (GeoB2107-3) off southern Brazil, *Quat. Sci. Rev.*, 172, 55–71,
497 doi:10.1016/j.quascirev.2017.06.028, 2017.

498 Hendry, K. R., Robinson, L. F., Meredith, M. P., Mulitza, S., Chiessi, C. M. and Arz, H.: Abrupt
499 changes in high-latitude nutrient supply to the Atlantic during the last glacial cycle, *Geology*,
500 40(2), 123–126, doi:10.1130/G32779.1, 2012.

501 Ito, R. G., Garcia, C. A. E. and Tavano, V. M.: Net sea-air CO₂ fluxes and modelled pCO₂ in the
502 southwestern subtropical Atlantic continental shelf during spring 2010 and summer 2011, *Cont.*
503 *Shelf Res.*, 119, 68–84, doi:10.1016/J.CSR.2016.03.013, 2016.

504 Juggins, S.: C2 user guide: Software for ecological and palaeoecological data analysis and
505 visualization, 2003.

506 Kucera, M., Rosell-Melé, A., Schneider, R., Waelbroeck, C. and Weinelt, M.: Multiproxy approach for
507 the reconstruction of the glacial ocean surface (MARGO), *Quat. Sci. Rev.*, 24(7–9), 813–819,
508 doi:10.1016/j.quascirev.2004.07.017, 2005a.

509 Kucera, M., Weinelt, M., Kiefer, T., Pflaumann, U., Hayes, A., Weinelt, M., Chen, M.-T., Mix, A. C.,
510 Barrows, T. T., Cortijo, E., Duprat, J., Juggins, S. and Waelbroeck, C.: Reconstruction of sea-
511 surface temperatures from assemblages of planktonic foraminifera: multi-technique approach
512 based on geographically constrained calibration data sets and its application to glacial Atlantic
513 and Pacific Oceans, *Quat. Sci. Rev.*, 24(7–9), 951–998, doi:10.1016/j.quascirev.2004.07.014,
514 2005b.

515 Lantzsch, H., Hanebuth, T. J. J., Chiessi, C. M., Schwenk, T. and Violante, R. A.: The high-supply,
516 current-dominated continental margin of southeastern South America during the late Quaternary,
517 *Quat. Res.*, 81(02), 339–354, doi:10.1016/j.yqres.2014.01.003, 2014.

518 Lessa, D. V. de O., Portilho-Ramos, R. C., Barbosa, C. F., da Silva, A. R., Belem, A., Turcq, B.,
519 Albuquerque, A. L. and Ramos, R. P.: Planktonic foraminifera in the sediment of a western
520 boundary upwelling system off Cabo Frio, Brazil, *Mar. Micropaleontol.*, 106, 55–68,

521 doi:10.1016/j.marmicro.2013.12.003, 2014.

522 Lessa, D. V. O., Santos, T. P., Venancio, I. M. and Albuquerque, A. L. S.: Offshore expansion of the
523 Brazilian coastal upwelling zones during Marine Isotope Stage 5, *Glob. Planet. Change*,
524 158(September), 13–20, doi:10.1016/j.gloplacha.2017.09.006, 2017.

525 Lisiecki, L. E. and Stern, J. V.: Regional and global benthic D18 O stacks for the last glacial cycle,
526 *Paleoceanography*, 31(10), 1368–1394, doi:10.1002/2016PA003002, 2016.

527 Locarnini R.A., Mishonov A.V., Antonov J.I., Boyer T.P., Garcia O.H.E., Baranova O.K., Zweng
528 M.M.: World ocean database 2009, vol 1: temperature. US government printing office,
529 Washington,DC., 2009.

530 Martínez-Méndez, G., Zahn, R., Hall, I. R., Peeters, F. J. C., Pena, L. D., Cacho, I. and Negre, C.:
531 Contrasting multiproxy reconstructions of surface ocean hydrography in the Agulhas Corridor
532 and implications for the Agulhas Leakage during the last 345,000 years, *Paleoceanography*,
533 25(4), PA4227, doi:10.1029/2009PA001879, 2010.

534 Matsumoto, K., Chase, Z. and Kohfeld, K.: Different mechanisms of silicic acid leakage and their
535 biogeochemical consequences, *Paleoceanography*, 29(3), 238–254, doi:10.1002/2013PA002588,
536 2014.

537 Mohtadi, M., Max, L., Hebbeln, D., Baumgart, A., Krück, N. and Jennerjahn, T.: Modern
538 environmental conditions recorded in surface sediment samples off W and SW Indonesia:
539 Planktonic foraminifera and biogenic compounds analyses, *Mar. Micropaleontol.*, 65(1–2), 96–
540 112, doi:10.1016/j.marmicro.2007.06.004, 2007.

541 Möller, O. O., Piola, A. R., Freitas, A. C. and Campos, E. J. D.: The effects of river discharge and
542 seasonal winds on the shelf off southeastern South America, *Cont. Shelf Res.*, 28(13), 1607–
543 1624, doi:10.1016/j.csr.2008.03.012, 2008.

544 Morey, A. E., Mix, A. C. and Pisias, N. G.: Planktonic foraminiferal assemblages preserved in surface
545 sediments correspond to multiple environment variables, *Quat. Sci. Rev.*, 24(7–9), 925–950,
546 doi:10.1016/j.quascirev.2003.09.011, 2005.

547 Mortlock, R. A., Charles, C. D., Froelich, P. N., Zibello, M. A., Saltzman, J., Hays, J. D. and Burckle,
548 L. H.: Evidence for lower productivity in the Antarctic Ocean during the last glaciation, *Nature*,
549 351(6323), 220–223, doi:10.1038/351220a0, 1991.

550 Muller-Karger, F. E., Varela, R., Thunell, R., Luerssen, R., Hu, C. and Walsh, J. J.: The importance of
551 continental margins in the global carbon cycle, *Geophys. Res. Lett.*, 32(1), 1–4,
552 doi:10.1029/2004GL021346, 2005.

553 Paillard, D., Labeyrie, L. and Yiou, P.: Macintosh Program performs time-series analysis, *Eos*,
554 *Transactions American Geophysical Union*, 77(39), 379, doi:10.1029/96EO00259, 1996.

555 Peeters, F. J. C., Brummer, G. J. A. and Ganssen, G.: The effect of upwelling on the distribution and
556 stable isotope composition of *Globigerina bulloides* and *Globigerinoides ruber* (planktic
557 foraminifera) in modern surface waters of the NW Arabian Sea, *Glob. Planet. Change*, 34, 269–
558 291, doi:10.1016/S0921-8181(02)00120-0, 2002.

559 Petró, S. M., Pivel, M. A. G., Coimbra, J. C. and Mizusaki, A. M. P.: Paleoceanographic changes
560 through the last 130 ka in the western South Atlantic based on planktonic Foraminifera, *Rev.*

561 Bras. Paleontol., 19(1), 3–14, doi:10.4072/rbp.2016.1.01, 2016.

562 Portilho-Ramos, R. C., Ferreira, F., Lago, L. C., Da Silva, A. G. V., Jaworski, K. S. and Toledo, M. B.:
563 *Globorotalia crassaformis* optimum event: a new late Quaternary biostratigraphic marker for the
564 southeastern Brazilian margin, *Palaios*, 29(11), 578–593, doi:10.2110/palo.2013.097, 2014a.

565 Portilho-Ramos, R. C., Barbosa, C. F. and Rios-Netto, A. M.: Planktonic foraminiferal variations in the
566 southwestern Atlantic since the last glacial-interglacial cycle, *Palaios*, 29(1), 38–44,
567 doi:10.2110/palo.2012.104, 2014b.

568 Portilho-Ramos, R. C., Ferreira, F., Calado, L., Frontalini, F. and de Toledo, M. B.: Variability of the
569 upwelling system in the southeastern Brazilian margin for the last 110,000years, *Glob. Planet.*
570 *Change*, 135, 179–189, doi:10.1016/j.gloplacha.2015.11.003, 2015.

571 Reimer, P. J., Bard, E., Bayliss, A., Beck, J. W., Blackwell, P. G., Ramsey, C. B., Buck, C. E., Cheng,
572 H., Edwards, R. L., Friedrich, M., Grootes, P. M., Guilderson, T. P., Haflidason, H., Hajdas, I.,
573 Hatté, C., Heaton, T. J., Hoffmann, D. L., Hogg, A. G., Hughen, K. A., Kaiser, K. F., Kromer, B.,
574 Manning, S. W., Niu, M., Reimer, R. W., Richards, D. A., Scott, E. M., Southon, J. R., Staff, R.
575 A., Turney, C. S. M. and van der Plicht, J.: IntCal13 and Marine13 Radiocarbon Age Calibration
576 Curves 0–50,000 Years cal BP, *Radiocarbon*, 55(04), 1869–1887,
577 doi:10.2458/azu_js_rc.55.16947, 2013.

578 Rodrigues, R. R. and Lorenzetti, J. A.: A numerical study of the effects of bottom topography and
579 coastline geometry on the Southeast Brazilian coastal upwelling, *Cont. Shelf Res.*, 21(4), 371–
580 394, doi:10.1016/S0278-4343(00)00094-7, 2001.

581 Rodrigues, S. V., Marinho, M. M., Jonck, C. C. C., Gonçalves, E. S., Brant, V. F., Paranhos, R.,
582 Curbelo, M. P. and Falcão, A. P.: Phytoplankton community structures in shelf and oceanic
583 waters off southeast Brazil (20°–25°S), as determined by pigment signatures, *Deep. Res. Part I*
584 *Oceanogr. Res. Pap.*, 88, 47–62, doi:10.1016/j.dsr.2014.03.006, 2014.

585 Salgueiro, E., Naughton, F., Voelker, A. H. L., Abreu, L. De and Alberto, A.: Past circulation along the
586 western Iberian margin : a time slice vision from the Last Glacial to the Holocene, *Quat. Sci.*
587 *Rev.*, 106, doi:10.1016/j.quascirev.2014.09.001, 2014.

588 Santos, T. P., Lessa, D. O., Venancio, I. M., Chiessi, C. M., Mulitza, S., Kuhnert, H., Govin, A.,
589 Machado, T., Costa, K. B., Toledo, F., Dias, B. B. and Albuquerque, A. L. S.: Prolonged
590 warming of the Brazil Current precedes deglaciations, *Earth and Planetary Science Letters*, 463,
591 1–12, doi:10.1016/j.epsl.2017.01.014, 2017.

592 Sarmiento, J. L., Gruber, N., Brzezinski, M. A. and Dunne, J. P.: High-latitude controls of thermocline
593 nutrients and low latitude biological productivity., *Nature*, 427(6969), 56–60,
594 doi:10.1038/nature10605, 2004.

595 Sautter, L. R. and Thunell, R. C.: Planktonic foraminiferal response to upwelling and seasonal
596 hydrographic conditions; sediment trap results from San Pedro Basin, Southern California Bight,
597 *J. Foraminifer. Res.*, 21(4), 347–363, doi:10.2113/gsjfr.21.4.347, 1991.

598 Schiebel, R. and Hemleben, C.: Ecology, in *Planktic Foraminifers in the Modern Ocean*, pp. 209–230,
599 Springer Berlin Heidelberg, Berlin, Heidelberg., 2017.

600 Stainforth, R. M., Lamb, J. L., Luterbacher, H., Beard, J. H. and Jeffords, R. M.: Cenozoic Planktonic

601 Foraminiferal Zonation and Characteristics of Index Formsle, The Paleontological Institute, The
602 University of Kansas, Kansas. [online] Available from: <http://hdl.handle.net/1808/3836>
603 (Accessed 14 March 2017), 1975.

604 Tessin, A. C. and Lund, D. C.: Isotopically depleted carbon in the mid-depth South Atlantic during the
605 last deglaciation, *Paleoceanography*, 28(2), 296–306, doi:10.1002/palo.20026, 2013.

606 Thunell, R. and Sautter, L. R.: Planktonic foraminiferal faunal and stable isotopic indices of upwelling:
607 a sediment trap study in the San Pedro Basin, Southern California Bight, *Geol. Soc. London,*
608 *Spec. Publ.*, 64(1), 77–91, doi:10.1144/GSL.SP.1992.064.01.05, 1992.

609 Toledo, F. A. L., Cachão, M., Costa, K. B. and Pivel, M. A. G.: Planktonic foraminifera, calcareous
610 nannoplankton and ascidian variations during the last 25 kyr in the Southwestern Atlantic: A
611 paleoproductivity signature?, *Mar. Micropaleontol.*, 64(1–2), 67–79,
612 doi:10.1016/j.marmicro.2007.03.001, 2007.

613 Turner, J. T.: Zooplankton fecal pellets, marine snow, phytodetritus and the ocean’s biological pump,
614 *Prog. Oceanogr.*, 130, 205–248, doi:10.1016/j.pocean.2014.08.005, 2015.

615 de Vargas, C., Bonzon, M., Rees, N. W., Pawlowski, J. and Zaninetti, L.: A molecular approach to
616 biodiversity and biogeography in the planktonic foraminifer *Globigerinella siphonifera*
617 (d’Orbigny), *Mar. Micropaleontol.*, 45(2), 101–116, doi:10.1016/S0377-8398(02)00037-3, 2002.

618 Volbers, A. N. A. and Henrich, R.: Calcium carbonate corrosiveness in the South Atlantic during the
619 Last Glacial Maximum as inferred from changes in the preservation of *Globigerina bulloides*: A
620 proxy to determine deep-water circulation patterns?, *Mar. Geol.*, 204, 43–57, doi:10.1016/S0025-
621 3227(03)00372-4, 2004.

622 Waelbroeck, C., Labeyrie, L., Michel, E., Duplessy, J. C., McManus, J. F., Lambeck, K., Ballon, E.
623 and Labracherie, M.: Sea-level and deep water temperature changes derived from benthic
624 foraminifera isotopic records, *Quat. Sci. Rev.*, 21(1–3), 295–305, doi:10.1016/S0277-
625 3791(01)00101-9, 2002.

626 Wang, D., Gouhier, T. C., Menge, B. A. and Ganguly, A. R.: Intensification and spatial
627 homogenization of coastal upwelling under climate change, *Nature*, 518(7539), 390–394,
628 doi:10.1038/nature14235, 2015.

629 Wang, X., Auler, A. S., Edwards, R. L., Cheng, H., Ito, E., Wang, Y., Kong, X. and Solheid, M.:
630 Millennial-scale precipitation changes in southern Brazil over the past 90,000 years, *Geophys.*
631 *Res. Lett.*, 34(23), L23701, doi:10.1029/2007GL031149, 2007.

Depth (cm)	¹⁴ C age (yr)	1 sigma error (yr)	Calibrated age (cal ka BP)	1 sigma error (yr)	Notes	$\delta^{18}\text{O}$ tie-points	Estimated error	Reference
10	4140	80	4228	283				Tessin and Lund (2013)
18	6970	20	7463	201				Tessin and Lund (2013)
26	9895	25	10784	233				Tessin and Lund (2013)
30	10555	25	11795	298				Tessin and Lund (2013)
34	11955	30	13454	195				Tessin and Lund (2013)
38	12870	30	14550	341				Tessin and Lund (2013)
42	13650	35	16001	390				Tessin and Lund (2013)
50	4190	15	4281	264	reversal			Tessin and Lund (2013)
54	14080	35	16569	338				Tessin and Lund (2013)
56	10000	60	10967	147	reversal			Portilho-Ramos et al. (2014)
58	10990	35	12371	273	reversal			Tessin and Lund (2013)
66	10790	25	12091	273	reversal			Tessin and Lund (2013)
74	18010	100	20922	282				Tessin and Lund (2013)
82	16120	80	18994	199	reversal			Tessin and Lund (2013)
90	18100	60	20975	282				Tessin and Lund (2013)
98	19020	70	22074	292				Tessin and Lund (2013)
190	32550	270	37946	312				Portilho-Ramos et al. (2014)
260						57614	3870	This study
350						70000	2260	This study

632 **Table 1:** Chronology of core JPC-17 obtained by accelerator mass spectrometry (AMS) ¹⁴C dating on planktonic foraminifera shells (Tessin and Lund, 2013; Portilho-Ramos
633 et al., 2014a) and stable oxygen isotope ($\delta^{18}\text{O}$) tie-points tuned to the LS16 stack from Lisiecki and Stern (2016).

634
635
636
637
638
639
640
641
642
643
644
645
646
647
648
649
650

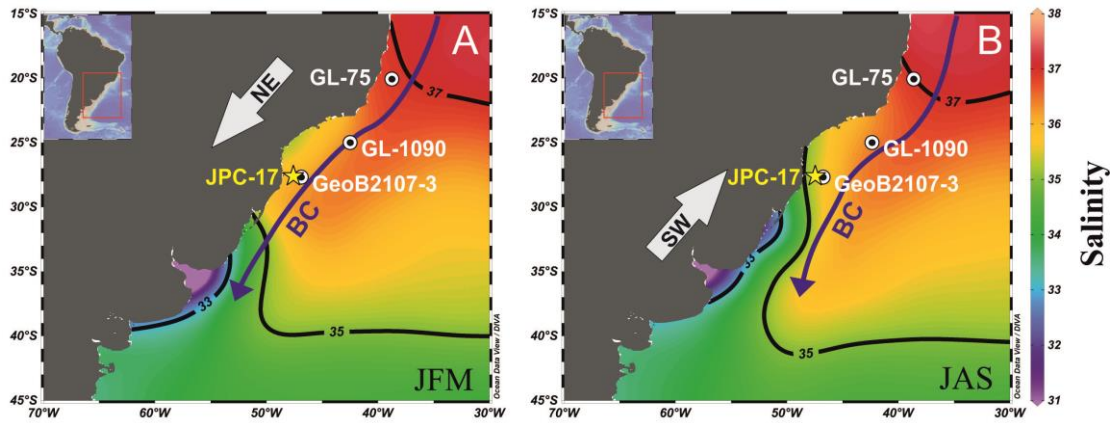
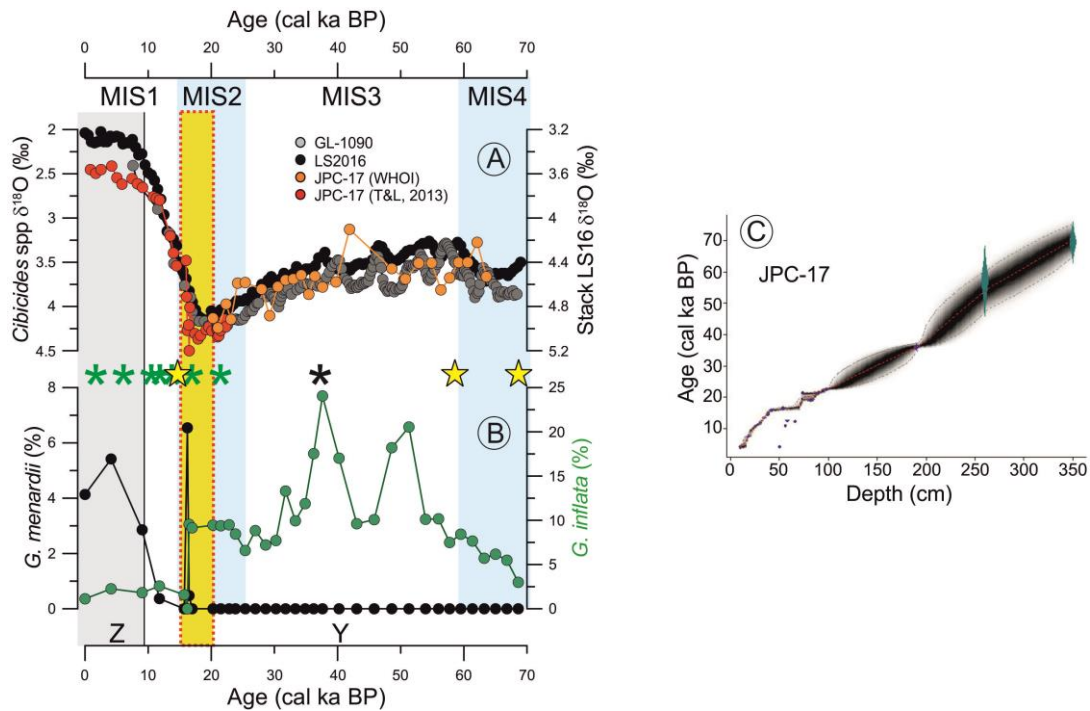


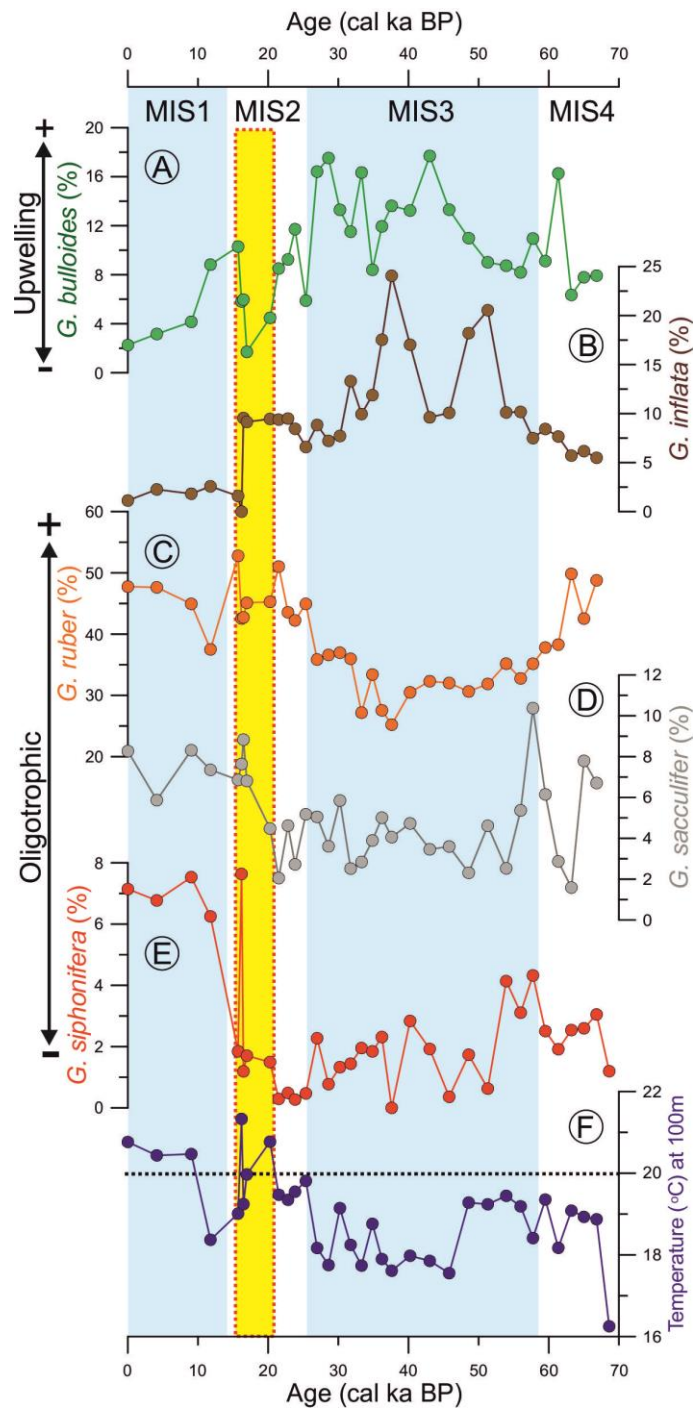
Figure 1: Surface salinity in southwestern Atlantic Ocean (Locarnini et al., 2010) during (A) austral summer (December-February, DJF) and (B) winter (June-August, JJA) showing the location of cores JPC-17 (this study), GeoB2107-3 (27°17'S; 46°45'W; Gu et al., 2017), GL-1090 (24°92'S; 42°51' W; Santos et al., 2017) and GL-75 (Portilho-Ramos et al., 2015). Blue arrows indicate the western boundary Brazil Current (BC) and the gray arrows show the regional prevailing alongshore wind direction (northeastern – NE and southwestern – SW). Figure created using the Ocean Data View software (ODV - version, 4.7.10., <http://odv.awi.de>, 2018).

651
 652
 653
 654
 655
 656
 657
 658
 659
 660
 661
 662
 663



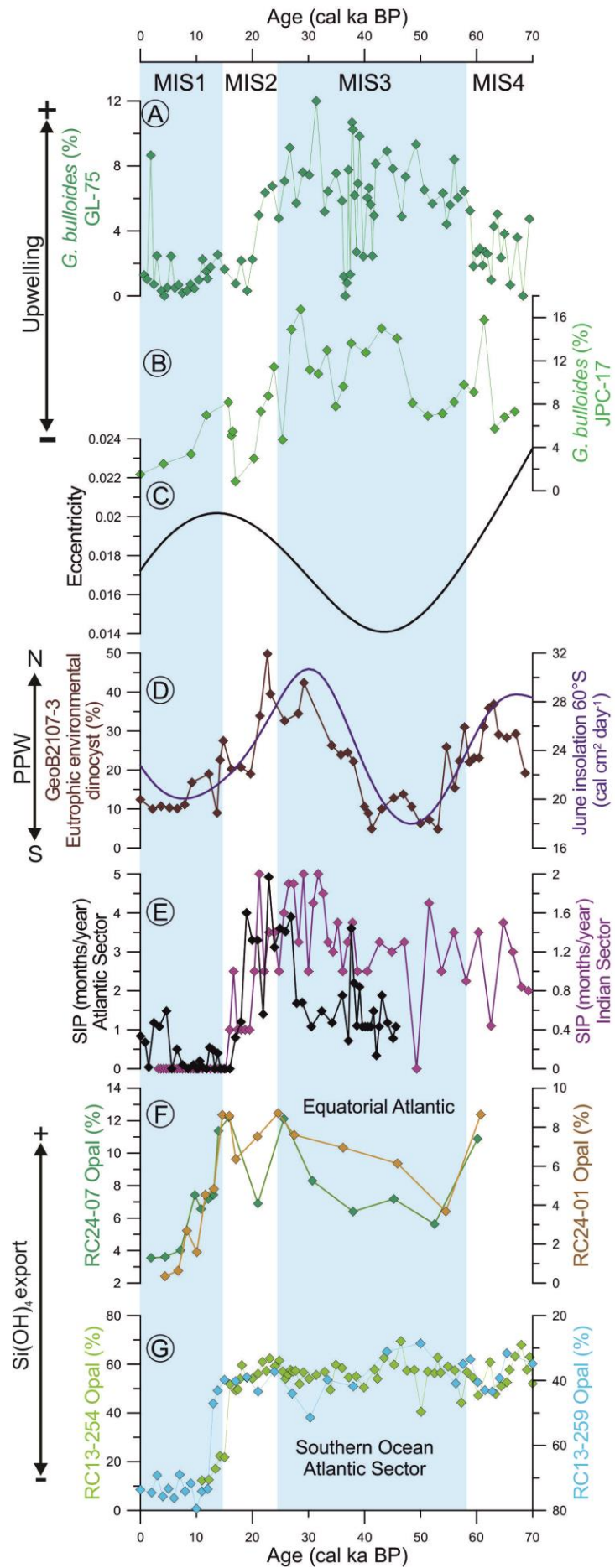
664 **Figure 2:** Age model of core JPC-17. (A) Comparison between the benthic foraminifera $\delta^{18}\text{O}$ record of
 665 JPC-17 (composed of published *Cibicidoides* spp. (Tessin and Lund, 2013; T&L, 2013) and unpublished
 666 *Cibicidoides* spp. data from Woods Hole Oceanographic Institution - WHOI) to the benthic foraminifera
 667 $\delta^{18}\text{O}$ record of core GL-1090 (Santos et al., 2017) as well as to the intermediate-depth South Atlantic
 668 benthic $\delta^{18}\text{O}$ stack LS16 (Lisiecki and Stern, 2016). Asterisks represent the calibrated radiocarbon ages
 669 published in (green) Tessin and Lund (2013) and (black) Portilho-Ramos et al. (2014b), while yellow
 670 stars represent the $\delta^{18}\text{O}$ tie-points shown in Table 2. (B) Abundance of the main biostratigraphical
 671 planktonic foraminifera species *Globorotalia menardii* and *Globorotalia inflata* from core JPC-17.
 672 Marine Isotopic Stages 1 to 4 (MIS1–4; MIS 2 and 4 indicated by vertical blue bars) are shown at the
 673 top, while letters Z (vertical grey bar) and Y in the bottom correspond to biostratigraphical biozones of
 674 Ericson and Wollin (1968). (C) Age-depth model based on Bacon v. 2.2 (Blaauw and Christeny, 2011).
 675 The symbols represent the positions of the calibrated AMS ^{14}C ages benthic $\delta^{18}\text{O}$ tie-points listed in
 676 Table 1. Error estimations of $\delta^{18}\text{O}$ tie-points follow Santos et al. (2017) that take into account the mean
 677 resolution of the JPC-17 benthic $\delta^{18}\text{O}$ record around the tie-point depth, the mean resolution of the
 678 reference curve around the tie-point age, a matching error visually estimated when defining tie-points
 679 and the absolute age error of the time-scale used for the reference record. The vertical yellow bar marks
 680 the interval with reversed radiocarbon ages listed in Table 1.

681
 682
 683
 684
 685
 686
 687
 688
 689
 690
 691
 692
 693
 694
 695
 696
 697
 698
 699
 700
 701
 702
 703
 704
 705
 706
 707
 708
 709
 710
 711



712 **Figure 3:** Relative abundance of planktonic foraminifera species and reconstructed subsurface
 713 temperature (100 m water depth) from core JPC-17 over the last 70 kyr. (A) Relative abundance of
 714 *Globigerina bulloides*, (B) *Globorotalia inflata*, (C) *Globigerinoides ruber*, (D) *Globigerinoides*
 715 *sacculifer* and (E) *Globigerinella siphonifera*. (F) Temperature at 100m water depth. Blue dashed line
 716 in (F) indicates the 20°C isotherm which defines the modern maximum temperature of South Atlantic
 717 Central Water (Castelao et al., 2004), the water mass entering the photic zone in the upwelling sites of
 718 the southern Brazilian margin. The vertical yellow bar marks the interval with reversed radiocarbon ages
 719 listed in Table 1.

720
721
722
723
724
725
726
727
728
729
730
731
732
733
734
735
736
737
738
739
740
741
742
743
744
745
746
747
748
749
750
751
752
753
754
755
756
757



758 **Figure 4:** Mechanism behind the variability of the productivity in the southern Brazilian margin over
759 the last 70 kyr. Abundance of upwelling indicator species *G. bulloides* from (A) core GL-75 (21°S)
760 (Portilho-Ramos et al., 2015) and (B) core JPC-17 (27°S) (this study). C. Eccentricity and austral summer
761 (January) insolation at 15°S (Berger and Loutre, 1991). (D) Abundance of dinoflagellate cysts from core
762 GeoB2107-3 (27°S) representing the influence of the Plata Plume Water in the southern Brazilian margin
763 (Gu et al., 2017) and austral winter (June) insolation at 65°S (Berger and Loutre, 1991). (E) Antarctic
764 sea ice presence (SIP) in the Atlantic Sector core TN057-13-PC4 (53°20'S; 5°10'W; Shemesh et al 2002)
765 and Indian Sector core SO136-111 (56°40'S; 160°14'W; Crosta et al., 2004) sectors of the Southern
766 Ocean derived from diatoms assemblage. (F) Opal content in Equatorial Atlantic upwelling off NW-
767 African cores RC14-01 (0.55°N; 13°65'W) and core RC24-07 (1°33'S; 11°92'W) (Bradtmilller et al.,
768 2007) as well as (G) in Atlantic sector of the Southern Ocean cores RC13-254 (48°34'S; 5°34'E) and
769 core RC13-259 (53°53'S; 4°56'W) as a proxy for silicic acid transport toward low latitudes (Mortlock
770 et al., 1991). Core RC13-254 is located to the north of the Antarctic Polar Zone (APZ) while core RC13-
771 254 is located to the south of the APZ. Note the inverted (RC13-259) axis in (F).